Crystal structure, XANES and charge distribution investigation of krennerite and sylvanite: analysis of Au-Te and Te-Te bonds in Au1–x Ag x Te2 group minerals

Ginga Kitahara, Akira Yoshiasa, Makoto Tokuda, Massimo Nespolo, Hidetomo Hongu, Koichi Momma, Ritsuro Miyawaki, Kazumasa Sugiyama

▶ **To cite this version:**

Ginga Kitahara, Akira Yoshiasa, Makoto Tokuda, Massimo Nespolo, Hidetomo Hongu, et al.. Crystal structure, XANES and charge distribution investigation of krennerite and sylvanite: analysis of Au-Te and Te-Te bonds in Au1–x Ag x Te2 group minerals. Acta Crystallographica Section B : Structural Science, Crystal Engineering and Materials [2014-..], 2022, 78 (2), pp.117-132. 10.1107/s2052520622000804 . hal-03633784

HAL Id: hal-03633784

https://hal.univ-lorraine.fr/hal-03633784

Submitted on 7 Apr 2022

HAL is a multi-disciplinary open access archive for the deposit and dissemination of scientific research documents, whether they are published or not. The documents may come from teaching and research institutions in France or abroad, or from public or private research centers.

L'archive ouverte pluridisciplinaire **HAL**, est destinée au dépôt et à la diffusion de documents scientifiques de niveau recherche, publiés ou non, émanant des établissements d'enseignement et de recherche français ou étrangers, des laboratoires publics ou privés.

electronic reprint

STRUCTURAL SCIENCE
CRYSTAL ENGINEERING
MATERIALS

ISSN: 2052-5206
journals.iucr.org/b

Crystal structure, XANES and charge distribution investigation of krennerite and sylvanite: analysis of Au—Te and Te—Te bonds in $Au_{1-x}Ag_xTe_2$ group minerals

Ginga Kitahara, Akira Yoshiasa, Makoto Tokuda, Massimo Nespolo, Hidetomo Hongu, Koichi Momma, Ritsuro Miyawaki and Kazumasa Sugiyama

Acta Cryst. (2022). B**78**, 117–132

IUCr Journals
CRYSTALLOGRAPHY JOURNALS ONLINE

Author(s) of this article may load this reprint on their own web site or institutional repository provided that this cover page is retained. Republication of this article or its storage in electronic databases other than as specified above is not permitted without prior permission in writing from the IUCr.

For further information see https://journals.iucr.org/services/authorrights.html

STRUCTURAL SCIENCE CRYSTAL ENGINEERING MATERIALS

ISSN 2052-5206

Crystal structure, XANES and charge distribution investigation of krennerite and sylvanite: analysis of Au—Te and Te—Te bonds in $Au_{1-x}Ag_xTe_2$ group minerals

Ginga Kitahara,[a]* Akira Yoshiasa,[a] Makoto Tokuda,[b] Massimo Nespolo,[c] Hidetomo Hongu,[a] Koichi Momma,[d] Ritsuro Miyawaki[d] and Kazumasa Sugiyama[b]

[a]Faculty of Advanced Science and Technology, Kumamoto University, Kumamoto, 860-8555, Japan, [b]Institute for Materials Research, Tohoku University, Sendai, 980-8577, Japan, [c]Université de Lorraine, CNRS, CRM2, Nancy, France, and [d]Department of Geology, National Science Museum of Japan, Tokyo, 169-0073, Japan. *Correspondence e-mail: galaxy.kitahara@gmail.com

Received 9 November 2021
Accepted 23 January 2022

Edited by M. Dusek, Academy of Sciences of the Czech Republic, Czech Republic

Keywords: Au–Te bond distances; effective coordination number (ECoN); charge distribution; krennerite; sylvanite; single-crystal structure analysis.

CCDC references: 2143949; 2149413

Supporting information: this article has supporting information at journals.iucr.org/b

The structure refinement and XANES study of two gold–silver–tellurides [$Au_{1+x}Ag_xTe_2$, krennerite (x = 0.11–0.13) and sylvanite (x = 0.29–0.31)] are presented and the structures are compared with the prototype structure of calaverite (x = 0.08–0.10). Whereas the latter is well known for being incommensurately modulated at ambient conditions, neither krennerite nor sylvanite present any modulation. This is attributed to the presence of relatively strong Te—Te bonds (bond distances < 2.9 Å) in the two minerals, which are absent in calaverite (bond distances > 3.2 Å). In both tellurides, trivalent gold occurs in slightly distorted square planar coordination, whereas monovalent gold, partly substituted by monovalent silver, presents a 2+2+2 coordination, corresponding to distorted rhombic bipyramids. The differentiation between bonding and non-bonding contacts is obtained by computation of the Effective Coordination Number (ECoN). The CHARge DIstribution (CHARDI) analysis is satisfactory for both tellurides but suggests that the Te—Te bond in the $[Te_3]^{2-}$ anion is not entirely homopolar. Both tellurides can therefore be described as Madelung-type compounds, despite the presence of Te–Te in both structures.

1. Introduction

Gold occurs primarily as a native metal and secondarily as gold solid-solution, in particular as tellurides, despite the fact that tellurium is a very rare element, whose upper crustal abundance is estimated to be 0.027 ± 0.003 p.p.m. (Hu & Gao, 2008). In these solid solutions, silver frequently substitutes for gold in various amounts. The binding of tellurium with noble metals such as gold and silver was attributed to the semi-metallic nature of tellurium. The presence of gold telluride minerals may render an ore refractory, the extent of this depends on the telluride mineral present and the mineralogical association (Zhang *et al.*, 2010).

Gold–silver tellurides are known from numerous localities. The IMA (International Mineralogical Association) officially recognizes several valid mineral species: for three of them the ratio (Au,Ag)/Te is $\frac{1}{2}$: calaverite ($AuTe_2$), sylvanite [$(Ag,Au)_2Te_4$], krennerite (Au_3AgTe_8); for muthmannite ($AgAuTe_2$) and empressite (AgTe) it is 1; for montbrayite (Au_2Te_3) it is $\frac{2}{3}$; for petzite (Ag_3AuTe_2) and hessite (Ag_2Te) it is 2; stunzite, instead, is non-stoichiometric ($Ag_{10.96}Te_7$). Despite their simple chemistry, the crystal structure of these minerals shows relatively complicated relations, which have been so far only partially elucidated (Tunell & Pauling, 1952;

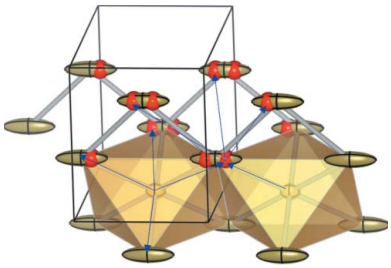

electronic reprint

Cabri, 1965; Bachechi, 1971; Schneider & Schulz, 1993; Bindi *et al.*, 2004; Dye & Smyth, 2012; Komuro & Nakata, 2016; Bindi & Keutsch, 2018). Hereafter we focus on gold–silver tellurides.

For gold ions, the stability of Au^{+} and Au^{3+} and the instability of Au^{2+} are known (Preiß *et al.*, 2017). The coexistence of Au^{+} and Au^{3+} is assumed in the $AuTe_2$ structure. The electron configuration of Au^{+} and Au^{3+} are [Xe] $4f^{14}$ $5d^{10}$ and [Xe] $4f^{14}$ $5d^{8}$, respectively. Linear covalent coordination is formed by *sp* hybridization and observed in several Au^{+} $5d^{10}$ compounds (Pauling, 1931; Elliott & Pauling, 1938; Cotton & Wilkinson, 1980; Hongu *et al.*, 2019*a*). Au^{3+} tends to form square planar covalent coordination, corresponding to the use of bonding orbitals formed by dsp^2 hybridization (Elliott & Pauling, 1938). In compounds, gold tends toward oxidation number +3 and silver toward oxidation number +1 (Tunell & Pauling, 1952).

Group V and VI elements (As, Sb, Bi, Se, Te), especially Te, form many minerals and compounds with gold, and are also frequently contained in gold minerals as subcomponents. Gold and platinum group compounds such as $AuSb_2$, $PtAs_2$ and $PdSe_2$ have pyrite-type MX_2 structures characterized by an X_2 unit with X—X covalent bond in the structure (Ewald & Friedrich, 1914; Tokuda *et al.*, 2019; Yoshiasa *et al.*, 2021). On the other hand, Te—Te covalent bonds do not systematically occur in tellurides; for instance, they are absent in petzite. Structures of calaverite, krennerite and sylvanite are related to the CdI_2-type structure. Regular arrangements of Te–Te units with covalent bonds are definitely present in krennerite and sylvanite (Tunell & Pauling, 1952). However, the existence of Te—Te covalent bonds in calaverite is unclear due to the statistical distribution of Te described by the split-atom model (Sueno *et al.*, 1979) or the large anisotropic mean-square distribution (MSD) (Schutte & de Boer, 1988; Reithmayer *et*

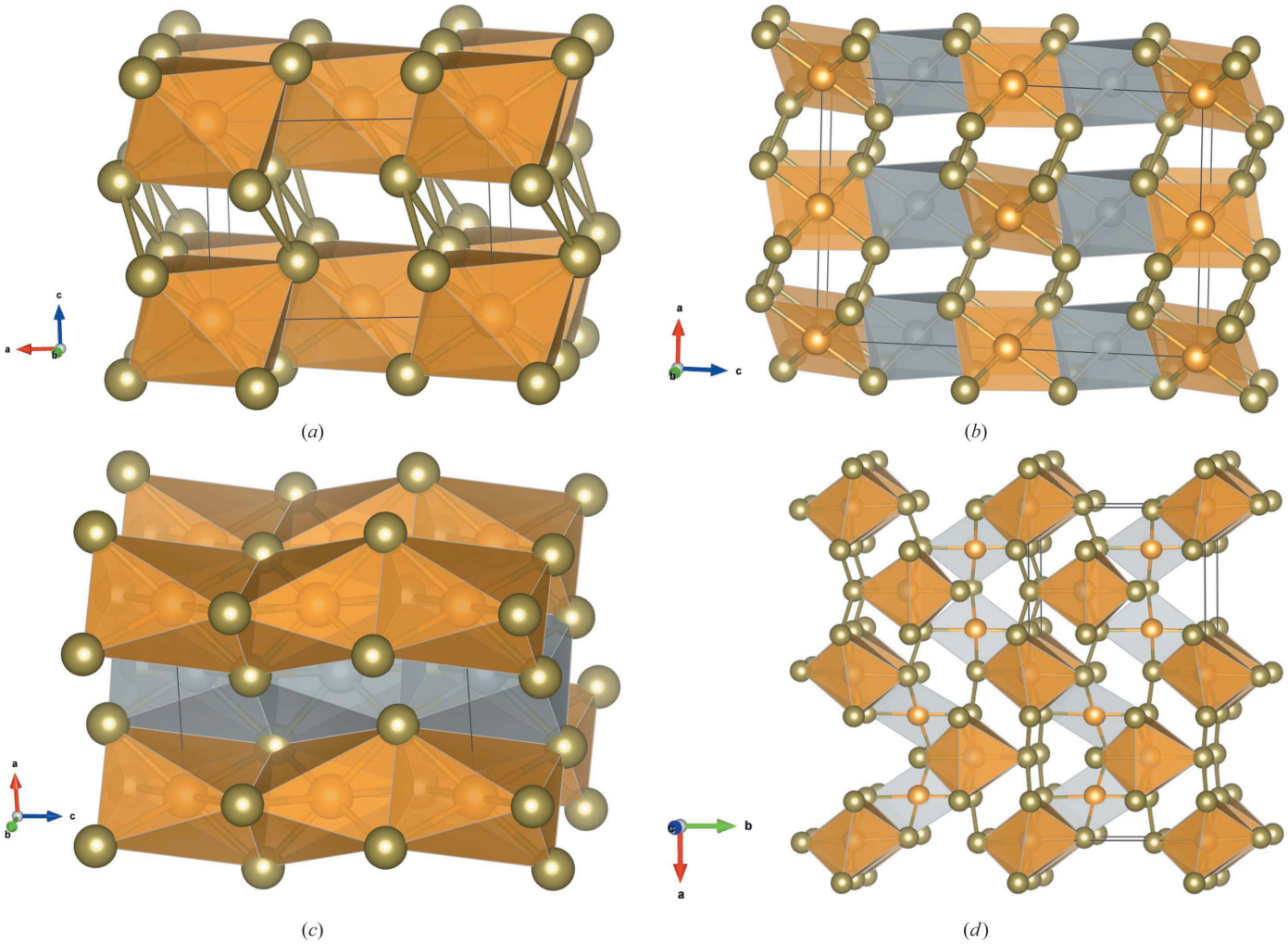

Figure 1
Comparison of the structures of calaverite (*a*), sylvanite (*b*), muthmannite (*c*) and krennerite (*d*). Gold and silver atoms are represented by the corresponding colour, tellurium is dark-olive-green. In the structure of sylvanite two types of polyhedra for Au^{3+} (slightly distorted square planar coordination) and Au^{+}/Ag^{+} (highly distorted octahedron) alternate forming sheets that are held together by Te—Te bonds much stronger than those in calaverite. The structure of muthmannite is built on edge-sharing highly distorted rhombic bipyramids centred on Au^{+} and on Ag^{+}, similar to those in calaverite, forming a three-periodic structure without Te—Te bonds. In the structure of krennerite two of the three sites host gold and silver, whereas the third site is occupied by gold alone. These corresponding polyhedra form zigzag sheets that are held together by strong Te—Te bonds similar to those found in sylvanite. This and the following structural figures were drawn with *VESTA* (Momma & Izumi, 2011).

electronic reprint

al., 1993). The shortest Te–Te distance of 3.20 Å in the average calaverite structure (Tunell & Pauling, 1952; Reithmayer *et al.*, 1993) is about 0.5 Å longer than those in krennerite and sylvanite, and corresponds to non-bonding contacts. The local coordination environment of Te—Te bond in sylvanite resemble to those in the pyrite-type compounds. One of the aims of this study is to reconfirm the existence of $[Te]_3$ and $[Te]_2$ units, as well as isolated tellurium (formally Te^{2-} ion) (Tunell & Pauling, 1952; Pertlik, 1984*b*) in the $Au_{1-x}Ag_xTe_2$ minerals using both diffraction and XAFS experiments.

Calaverite, krennerite and sylvanite have metallic lustre and are electrical conductors (Tunell & Pauling, 1952). Pure $AuTe_2$ exhibits super-conduction at low temperature (Kitagawa *et al.*, 2013). Petzite has excellent thermoelectric properties due to its low thermal conductivity and high electrical conductivity (Young *et al.*, 2000). Researches have been conducted in recent years to elucidate the mechanism behind the interesting physical properties of these compounds. These gold tellurides are brittle; krennerite and sylvanite have each one perfect cleavage.

In this study, we have performed structural analysis of krennerite and sylvanite samples with different chemical composition from the published ones and clarified the detailed structure, site occupancy in each site and bonding character especially for the Te atoms. We also note the systematic changes in the coordination environment and bond length of each atom among calaverite, krennerite and sylvanite. Au L_{III}-edge and Te *K*-edge XANES measurements have revealed similarities of electronic structures of these minerals. We reconsider the incommensurate modulation of calaverite by comparing the calaverite, krennerite and sylvanite structures. In particular, we discuss the likely causes of the presence of the incommensurate phase in calaverite, and its absence in sylvanite, where the presence of strong covalent bonds and of monovalent silver seem to make the modulation unnecessary. Understanding the bonding character between heavy chalcogen (heavy pnictogen) and metal elements, as well as the Debye temperature of these materials, may lead to the elucidation of the formation process of gold and platinum group minerals.

2. Real structures of tellurides

The crystal structures of these tellurides are far from simple, showing unique ordered structures or incommensurate modulation under ambient conditions (Sueno *et al.*, 1979; Schutte & de Boer, 1988; Reithmayer *et al.*, 1993; Bindi *et al.*, 2009). Calaverite shows incommensurate super-structure ordering only in certain compositional regions (Bindi *et al.*, 2009), whereas sylvanite and krennerite do not in any region. On the other hand, petzite Ag_3AuTe_2 is a compound with a defined silver-to-gold ratio (Thompson, 1949; Hongu *et al.*, 2019*a*), with distinct ordered positions for the silver and gold atoms, unlike calaverite, krennerite and sylvanite.

2.1. Structural relations in Au–Ag tellurides

The crystal structures of three Au–Ag tellurides [calaverite, sylvanite and muthmannite: Figs. 1(*a*), 1(*b*) and 1(*c*) respectively], are closely related but these relations have not been fully elucidated so far.

Calaverite occurs under high-pressure conditions as a distorted $P\bar{3}m1$ CdI_2-type structure that crystallizes in a space group of type *C*2/*m* (Reithmayer *et al.*, 1993). In this prototype structure [Fig. 1(*a*)] gold (Wyckoff position 2*a*, site-symmetry group of type 2/*m*) is coordinated by tellurium in a 2+4 rhombic bipyramid that can be described as a distorted octahedron, with Au—Te distances 2.6785 Å (2×) and 2.9711 Å (4×) and basal Te—Au—Te angles of 95.74 and 82.26°. Te–Te contacts at about 3.2 Å seem too weak to be considered as chemicals bonds capable to held together sheets of rhombic bipyramids; however, the real structure of calaverite is incommensurately modulated and the modulation induces the breaking up of zigzag chains and the formation of isolated Te_2 dimers with a short interatomic distance of 2.88 Å (Janner & Dam, 1989). The structure of sylvanite [Fig. 1(*b*)] presents Au^{3+} (Wyckoff position 4*a*, site-symmetry group of type $\bar{1}$)[1] in slightly distorted square planar coordination and Au^+/Ag^+ (Wyckoff position 4*e*, site-symmetry group of type 2) in a highly distorted octahedron corresponding to a 2+2+2 coordination. The two types of polyhedra alternate forming sheets, which are held together by Te—Te bonds which are much stronger than those in calaverite, the distance being shorter than 2.9 Å. The structure of muthmannite is significantly different, built on edge-sharing highly distorted rhombic bipyramids centred on Au^+ and on Ag^+, (all with site-symmetry group of type 2/*m*) similar to those in calaverite, forming a non-modulated structure without Te—Te bonds. Despite the differences in the coordination, a definite relation can be found among them, as shown in the following two sections.

The structure of krennerite [Fig. 1(*d*)] shows a more complex relation with that of calaverite, namely as a cell-twin of calaverite (Van Tendeloo *et al.*, 1984). Krennerite with intermediate composition between calaverite and sylvanite is acentric orthorhombic, with 16 Te per unit cell. It was originally determined by Tunell & Ksanda (1936) and refined by Tunell & Murata (1950), Pertlik *et al.* (1984*b*) and Dye & Smyth (2012) in space group *Pma2*. Pertlik (1984*b*) noted the ordering of the Au and Ag among three distinct octahedral sites. Actually, in two of the three sites gold and silver substitute and the coordination polyhedra are distorted rhombic bipyramids, whereas the third site, occupied by gold alone, is in a slightly distorted square planar coordination. These polyhedra form zigzag sheets that are held together by strong Te—Te bonds similar to those found in sylvanite.

The crystal structure of montbrayite (Bachechi, 1971) was solved by X-ray diffraction with a precession camera and visual inspection of intensities recorded on a photographic

[1] The multiplicity of the Wyckoff positions in the unconventional *B*2/*e* setting of the space group is doubled with respect to the corresponding multiplicity in the convention *P*2/*c* setting because of the addition *B*-centring.

electronic reprint

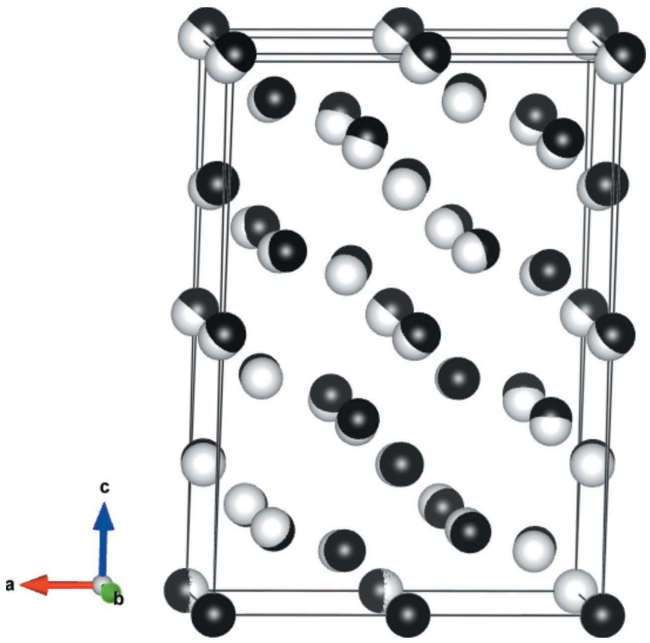

Figure 2
Comparison of the structures of calaverite (white atoms) in the *B*2/*m* setting and sylvanite (black atoms) in the *B*2/*e* setting.

film, without absorption correction, and an agreement factor $R1 = 0.23$. The quality of the refinement does not allow any reasonable comparison with other gold tellurides.

2.1.1. Calaverite versus sylvanite. The structure relation between the calaverite prototype and sylvanite can be shown by describing them in unconventional settings of their space groups.

The structure of sylvanite was reported by Tunell (1941) and Pertlik (1984*a*) in *P*2/*c*, with unit-cell parameters $a = 8.94$, $b = 4.48$, $c = 14.59$ Å, $\beta = 145.43°$, $V = 331.566$ Å^3, $Z = 4$. The unusually large value of the monoclinic angle suggests that the choice of the setting of the space group was not the most suitable one. Indeed, the ratio $c/2a$ is almost identical to $-\cos(\beta)$, showing that the lattice is almost exactly orthorhombic, when described in an unconventional *B*-centred setting. A change of the coordinate system to 2**a**+**c**,**b**,**c** leads to a *B*-centred unit cell whose parameters are $a = 10.15$, $b = 4.48$, $c = 14.59$ Å, $\beta = 90.75°$, $V = 663.132$ Å^3, $Z = 8$. In this setting, the Hermann–Mauguin symbol of the space group becomes *B*2/*e* (Nespolo & Aroyo, 2016).

Calaverite prototype structure has been reported in *C*2/*m* with unit-cell parameters $a = 7.189$, $b = 4.407$, $c = 5.069$ Å, $\beta = 89.96°$, $V = 160.596$ Å^3, $Z = 2$ (Reithmayer *et al.*, 1993). Comparison of the unit-cell parameters with those of sylvanite

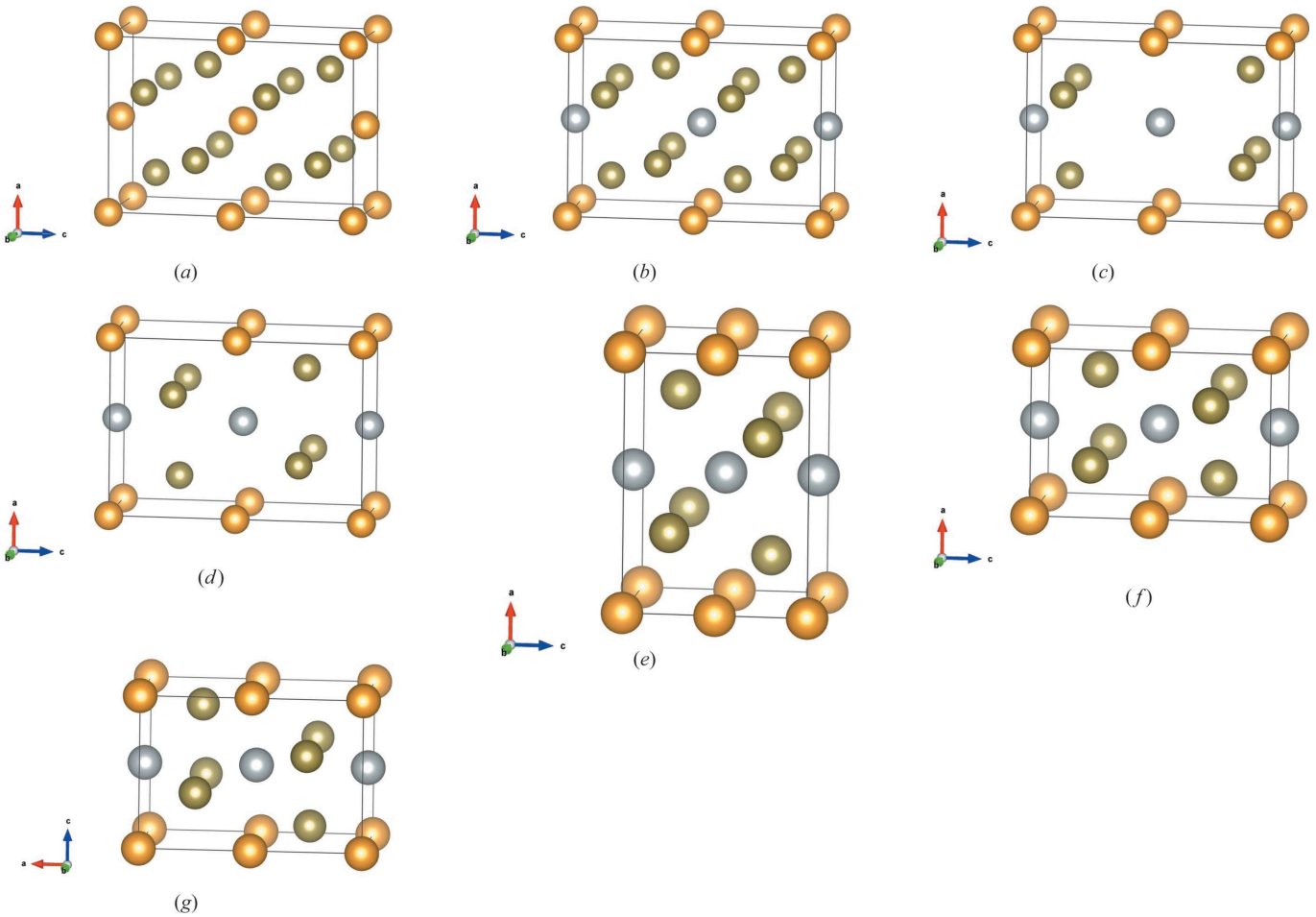

Figure 3
Step-by-step conversion of the structure of calaverite to that of muthmannite.

electronic reprint

Table 1
Chemical compositions for calaverite, krennerite and sylvanite used in this study.

	Calaverite (31 points data)		Krennerite (24 points data)		Sylvanite (26 points data)	
wt%	Average	Range	Average	Range	Average	Range
Au	40.40 (38)	39.60–41.18	39.25 (31)	38.79–39.85	37.18 (34)	31.66–33.08
Ag	2.12 (14)	1.85–2.38	2.85 (12)	2.61–3.07	7.66 (15)	7.36–7.96
Te	57.18 (26)	56.81–57.80	57.63 (26)	57.19–58.09	60.04 (42)	59.17–60.70
Total	99.70 (53)	99.01–100.75	99.73 (48)	99.01–100.86	99.87 (56)	99.08–100.98

	Calaverite		Krennerite		Sylvanite	
mol% (Te = 2)	Average	Range	Average	Range	Average	Range
Au	0.915 (8)	0.896–0.939	0.882 (6)	0.869–0.900	0.694 (10)	0.683–0.724
Ag	0.088 (6)	0.077–0.099	0.117 (5)	0.107–0.126	0.302 (6)	0.291–0.313
Total	1.003 (10)		1.000 (8)		0.996 (13)	

in the *B*2/*e* setting suggests that a relation between these two structures may be found by a change of coordinate system to $-2\mathbf{c},\mathbf{b},2\mathbf{a}$, leading to a four times larger unit cell (V = 642.383 Å^3, Z = 8) with unusual centring vectors $\frac{1}{2}$,0,0; 0,0,$\frac{1}{2}$, 0,$\frac{1}{2}$,$\pm\frac{1}{4}$, $\frac{1}{2}$,$\frac{1}{2}$,$\pm\frac{1}{4}$, $\frac{1}{2}$,0,$\frac{1}{2}$. There is no conventional way of indicating such an unusual unit cell; in a case like this, the letter X is commonly used in the literature, accompanied by the specification of the centring vectors. Alternatively, calaverite prototype can be described in the isomorphic subgroup *B*2/*m* of index 4, by adding to the larger *B*-centred unit cell the atoms that are actually generated by the unusual translations. The comparison actually requires an additional step: a twofold rotation about the *c*-axis of calaverite (originally *a* axis, in the *C*2/*m* setting). Once the comparison is performed in these two settings, the correspondence of the atomic sites is almost perfect (Fig. 2), if one ignores the 50% replacement of Au by Ag.

2.1.2. Calaverite versus muthmannite. The structure of muthmannite was reported by Bindi & Cipriani (2004) in space group *P*2/*m*, with cell parameters a = 5.124, b = 4.419, c = 7.437 Å, β = 89.96°. Despite the closeness of the cell parameters (apart from a swapping of the *a* and *c* axes), the relation with the structure of the calaverite prototype is less straightforward than in the case of sylvanite and can be pointed out through the following steps.

(1) Describe the structure of calaverite in a unit cell with doubled *c* axis, which corresponds to an isomorphic subgroup of index 2 [Fig. 3(*a*)].

(2) Replace the gold atom at the centre of the body as well as at the centre of the *C*-face by silver; this corresponds to further lowering the symmetry to an isomorphic subgroup of index 4 of the group of calaverite [Fig. 3(*b*)].

(3) Remove Te2 from the structure of calaverite, modifying therefore the ratio (Au,Ag)/Te from $\frac{1}{2}$ to 1 [Fig. 3(*c*)].

(4) Move Te1 atom along the *c* axis, at $z = \frac{1}{4}$ and $z = \frac{3}{4}$ [Fig. 3(*d*)].

(5) Shrink the *c* unit-cell parameter close to its original value [Fig. 3(*e*)].

(6) Swap the *a* and *c* axes [Fig. 3(*f*)].

Once these modification are applied to the structure of calaverite prototype, the relation with muthmannite [Fig. 3(*g*)] becomes evident.

3. Experimental

3.1. Specimens and chemical analyses

Three single crystals with metallic lustre and steel yellow colour were used in this study.

(1) Calaverite $Au_{0.915}Ag_{0.875}Te_2$, obtained from Lake View Mine, Golden Mile, Kalgoorlie, Australia (Kumamoto University, C133-calaverite-200906), used only for XANES measurement.

(2) Krennerite $Au_{0.882}Ag_{0.117}Te_2$, from Stratton Mine, Cripple Creek, Colorado, USA (NSM-MF 16988 of the National Museum of Nature and Science in Japan).

(3) Sylvanite $Au_{0.694}Ag_{0.302}Te_2$, from Emperor Mine, Vatukoula, Viti Levu, Fiji (Kumamoto University, C133-sylvanite-201001b).

The chemical composition of large single crystals with size of several millimetres was determined by a Jeol scanning electron microscope (SEM, JSM-7001F operated by 15 kV, 1.0 nA) equipped with Oxford energy-dispersive X-ray spectroscopy (EDS, Aztec SYSTEM). The variation of the Au and Ag molar ratio among numerous analysis points in each specimen was less than a few per cent (Table 1). Impurities such as copper, arsenic and antimony were below the detection threshold.

3.2. Single crystal X-ray diffraction experiments and structure refinements

We have collected single crystal X-ray diffraction data from krennerite and sylvanite with a Rigaku XtaLAB Synergy-S diffractometer with a HyPix-6000 detector. Data corrections for Lorentz and polarization effects, and for the absorption were carried out using *CrysAlisPro* (Rigaku OD, 2017). Data reduction resulted in R_{int} = 0.040 for krennerite and R_{int} = 0.045 for sylvanite which, although somewhat high, are not unusual for samples containing heavy atoms like ours.

Independent reflection numbers of 4231 and 2105 for krennerite and sylvanite, respectively, were used for refinement by full-matrix least-squares method. Details of the data collection are listed in Table 2. Structure refinement was performed using *JANA2020* (Petříček *et al.*, 2014). Refinement converged smoothly to $R1$ = 0.018 for krennerite and

electronic reprint

Table 2
Crystallographic data and data collection for krennerite and sylvanite.

	Krennerite	Sylvanite
Crystal data		
Chemical formula	$Au_{0.88}Ag_{0.12}Te_2$	$Au_{0.68}Ag_{0.32}Te_2$
Formula by site occupancy model	$(Au_{0.824(3)}Ag_{0.176(3)})$ $(Au_{0.680(3)}Ag_{0.320(3)})Au_2Te_8$	$Au(Au_{0.365(2)}\ Ag_{\ 0.635(2)})Te_4$
M_r	441.5	423.7
Crystal system, space group	Orthorhombic, *Pma*2 (No. 28)	Monoclinic, *B*2/*e* (No. 13)
Temperature (K)	293	
a, *b*, *c* (Å)	16.5937 (3), 8.8310 (1), 4.4786 (1)	10.136 (6), 4.4835 (1), 14.6444 (15)
α, β, γ (°)	90, 90, 90	90, 90.21 (3), 90
V (Å^3)	656.29 (2)	665.5 (4)
Z	8	8
Radiation type	Mo *K*α	Mo *K*α
μ (mm^{-1})	57.31	48.88
Crystal size (mm)	0.061 × 0.043 × 0.036	0.057 × 0.049 × 0.044
Data collection		
Diffractometer	Rigaku XtaLAB Synergy-S	
Absorption correction	Integration (Busing & Levy, 1957) or numerical absorption correction based on Gaussian integration over a multifaceted crystal model and empirical absorption correction using spherical harmonics, implemented in SCALE3 ABSPACK.	
T_{min}, T_{max}	0.110, 0.253	0.161, 0.262
No. of measured, independent and observed [$I > 3\sigma(I)$] reflections	48 587, 4231, 3779	22 154, 2105, 1844
R_{int}	0.040	0.045
$(\sin\theta/\lambda)_{max}$ (Å^{-1})	0.915	0.916
Refinement		
$R[F^2 > 2\sigma(F^2)]$, $wR(F^2)$, *S*	0.018, 0.039, 0.97	0.019, 0.043, 1.10
No. of reflections	4231	2105
No. of parameters	63	31
$\Delta\rho_{max}$, $\Delta\rho_{min}$ (e Å^{-3})	1.38, −4.03	1.55, −3.34
Absolute structure	1906 of Friedel pairs used in the refinement	–
Absolute structure parameter	−0.005 (2)	–

Table 3
Atomic coordinates and equivalent atomic displacement parameters for krennerite.

	Wyckoff position	Site-symmetry group	Site occupancy	*x*	*y*	*z*	U_{eq}
Au1	2*a*	..2	Au 0.826 (2) Ag 0.174 (2)	0.0	0.0	0.00370 (5)	0.01733 (6)
Au2	2*c*	*m*..	Au 0.676 (2) Ag 0.324 (2)	0.75	0.68062 (3)	0.01425 (6)	0.01917 (7)
Au3	4*d*	1	Au 1.0	0.873367 (9)	0.335341 (16)	0.51797 (4)	0.01359 (3)
Te1	2*c*	*m*..	Te 1.0	0.75	0.98428 (4)	0.05676 (8)	0.01388 (8)
Te2	2*c*	*m*..	Te 1.0	0.75	0.38115 (3)	0.13380 (8)	0.01273 (7)
Te3	4*d*	1	Te 1.0	−0.007587 (13)	0.30143 (2)	0.92478 (7)	0.01296 (5)
Te4	4*d*	1	Te 1.0	0.873352 (14)	0.63863 (3)	0.54224 (7)	0.01417 (6)
Te5	4*d*	1	Te 1.0	0.878789 (13)	0.03379 (3)	0.47508 (6)	0.01394 (6)

Table 4
Anisotropic atomic displacement parameters for krennerite.

	U_{11}	U_{22}	U_{33}	U_{23}	U_{13}	U_{12}
Au1	0.02020 (11)	0.01162 (9)	0.02017 (12)	0.00117 (6)	0	0
Au2	0.02106 (12)	0.01115 (10)	0.02529 (13)	0	0	−0.00022 (8)
Au3	0.01360 (5)	0.01049 (5)	0.01668 (5)	0.00052 (3)	−0.00257 (4)	−0.00081 (4)
Te1	0.01378 (12)	0.01146 (12)	0.01639 (16)	0	0	−0.00231 (10)
Te2	0.01223 (12)	0.01132 (12)	0.01463 (13)	0	0	0.00009 (10)
Te3	0.01301 (8)	0.01121 (9)	0.01467 (9)	−0.00017 (6)	−0.00025 (8)	0.00075 (8)
Te4	0.01436 (9)	0.01074 (9)	0.01741 (11)	−0.00044 (7)	0.00103 (7)	−0.00063 (8)
Te5	0.01398 (9)	0.01056 (8)	0.01727 (12)	−0.00013 (6)	0.00157 (7)	−0.00011 (7)

$R1$ = 0.019 for sylvanite; refinements of mixed occupancy Ag/Au at the 2*a* (Au1 site) and 2*c* (Au2 site) Wyckoff positions for krennerite and at the 2*e* (Au2 site) Wyckoff position for sylvanite give clear indication of isomorphic substitution of Ag for Au, confirming the preferential occupation of Au at the 4*d* (Au3 site) position for krennerite and at the 2*a* (Au1 site) position for sylvanite already reported in previous studies (Pertlik, 1984*a*,*b*; Dye & Smyth, 2012). The total amount of Ag

electronic reprint

Table 5
Atomic coordinates and equivalent atomic displacement parameters for sylvanite.

	Wyckoff position	Site-symmetry group	Site occupancy	x	y	z	U_{eq}
Au1	4*a*	1	Au 1.0	0.0	0.0	0.0	0.01388 (3)
Au2	4*e*	2	Au 0.3609 (19) Ag 0.6391 (19)	0.0	0.51632 (6)	0.25	0.02237 (7)
Te1	8*g*	1	Te 1.0	0.149428 (18)	0.02793 (4)	−0.149336 (13)	0.01469 (4)
Te2	8*g*	1	Te 1.0	0.140673 (16)	0.40559 (4)	0.095699 (12)	0.01390 (4)

Table 6
Anisotropic atomic displacement parameters for sylvanite.

	U_{11}	U_{22}	U_{33}	U_{23}	U_{13}	U_{12}
Au1	0.01228 (6)	0.01609 (6)	0.01326 (6)	−0.00270 (4)	0.00000 (4)	−0.00025 (4)
Au2	0.02203 (12)	0.02976 (14)	0.01535 (11)	0	0.00381 (8)	0
Te1	0.01250 (7)	0.01718 (7)	0.01440 (8)	0.00046 (5)	0.00073 (6)	0.00043 (5)
Te2	0.01205 (6)	0.01505 (7)	0.01460 (7)	−0.00012 (5)	−0.00031 (5)	−0.00115 (5)

Table 7
CHARDI results for krennerite.

q and *Q* are the formal and calculated charges (oxidation numbers), respectively.

Atom pair	Bond length (Å)	Arithmetic average	Weighted average	BW	Atom	ECoN	*q*	*Q*
Au/Ag1–Te3	2.6882 (2)×2	2.913	2.837	1.319	Au/Ag1	5.18	1.00	0.99
Au/Ag1–Te5	2.9311 (3)×2			0.806	Au/Ag2	5.07	1.00	1.00
Au/Ag1–Te5	3.1208 (4)×2			0.463	Au3	4.00	3.00	3.01
Au/Ag2–Te1	2.6884 (4)	2.936	2.850	1.343	Te1		−0.25	−0.26
Au/Ag2–Te2	2.6983 (4)			1.324	Te2		−1.75	−1.72
Au/Ag2–Te4	2.9658 (4)×2			0.761	Te3		−1.00	−0.98
Au/Ag2–Te4	3.1494 (4)×2			0.439	Te4		−1.00	−1.02
Ag3–Te5	2.6714 (3)	2.690	2.690	1.042	Te3		−1.00	−1.00
Ag3–Te4	2.6805 (3)			1.020				
Ag3–Te3	2.7039 (3)			0.969				
Ag3–Te2	2.7046 (3)			0.965				
Te1–Te5	2.8755 (4)×2							
Te3–Te4	2.8595 (4)							

Table 8
CHARDI results for sylvanite.

Atom pair	Bond length (Å)	Arithmetic average	Weighted average	BW		ECoN	*q*	*Q*
Au1–Te1	2.6677 (14)×2	2.899	2.683	1.036	Au1	3.99	3.00	3.00
Au1–Te2	2.6999 (10)×2			0.962	Au/Ag2	4.98	1.00	1.00
Au/Ag2–Te2	2.7220 (13)×2	2.962	2.862	1.296	Te1		−1.00	−0.98
Au/Ag2–Te1	2.9370 (11)×2			0.844	Te2		−1.00	−1.02
Au/Ag2	3.2257 (7)×2			0.350				
Te1–Te2	2.8281 (19)							

obtained from the refined cation occupancy is consistent with the chemical analysis. The higher peak in the difference Fourier map (1.554 e Å^{-3} or 1.62 e Å^{-3}, respectively) is not surprising, considering the difficulties in the absorption correction in samples containing heavy atoms.

The refinement of the krennerite structure model resulted in a Flack parameter of −0.005 (2). The absolute structure and the absence of inversion twinning were therefore confirmed. The crystal structure is drawn with *VESTA* (Momma & Izumi, 2011). The structure refinement data, atomic coordinates, anisotropic atomic displacement parameters and selected bond distances for krennerite and sylvanite are given in Tables 3, 4, 5, 6, 7 and 8.

3.3. XANES measurements

The XANES spectra near the Au L_{III}-edges and Te *K*-edges were measured in fluorescent mode on beamline NW-10A PF-AR, KEK, Tsukuba, Japan. The spectra of $Au(OH)_3$, $AuBr_3$, AuCl, $AuSb_2$ and metallic Au were also observed as reference compounds. The Au compounds were measured in a He atmosphere using different sample holders. The synchrotron radiation was monochromated with Si(311) double-crystal monochromator. X-ray energy calibration was performed by setting the copper metal pre-edge absorption peak to 8978.8 eV. The measurements were performed using the usual energy resolution to obtain sufficient X-ray flux. The resolution of photon energy is 0.1 eV. The details of the measure-

electronic reprint

ments and analyses are available in the literature (Tobase *et al.*, 2018; Yoshiasa *et al.*, 2018).

4. Results and discussion

4.1. Chemical compositions

Table 1 presents the chemical compositions of the samples analysed in this study. The range of x values for each mineral having the $Au_{1-x}Ag_xTe_2$ composition reported so far is shown in Fig. 4. In an experiment conducted by Cabri (1965), calaverite, krennerite, and sylvanite had composition regions of x = 0.00 to 0.11, x = 0.14 to 0.25, and x = 0.27 to 0.50, respectively. The structural analyses were performed in the range of x = 0.0 to 0.33 of $Au_{1-x}Ag_xTe_2$ as calaverite by Bindi *et al.* (2009). The incommensurately modulated structure of calaverite has been observed in the range $0 < x < 0.09$. No satellites have been detected for the Ag-rich members between x = 0.19 and x = 0.33 (Bindi *et al.*, 2009). Sueno *et al.* (1979) and Schutte & de Boer (1988) reported that the incommensurately modulated structure of calaverite is observed at least in the region of $0 < x < 0.15$. Krennerite with a range of composition $0.20 < x < 0.28$ has been reported by Van Tendeloo *et al.* (1984). In Fig. 4, the compositional region of the krennerite solid solution overlaps a considerable part with that of calaverite. The substitution region of Ag in calaverite and krennerite solid solutions seems to vary depending on the formation conditions.

In nature, the coexistence of calaverite and krennerite and of sylvanite and krennerite are common whereas the coexistence of calaverite and sylvanite is rare (Bindi *et al.*, 2005). The krennerite specimens analysed in this study have the composition of x = 0.12 (Table 1 and Fig. 4) and corresponds to the most Au-rich krennerite reported so far. Calaverite has been considered as a higher temperature phase in the system based on its occurrence and laboratory experiments (Cabri, 1965). Our sample of krennerite can be considered an ordered phase formed at a lower temperature than calaverite with the same composition. Due to the expanded substitution region of the ordered phase, our krennerite sample was probably formed at a lower temperature than the experimental conditions reported by Cabri (1965). The molar volume for our sylvanite (166.4 Å^3) is much smaller than that for calaverite with the same Ag contents [171.1 Å^3 for x = 0.32 estimated from Fig. 4(*d*) in Bindi *et al.* (2009)]. Therefore, sylvanite is here also considered a low-temperature phase of calaverite.

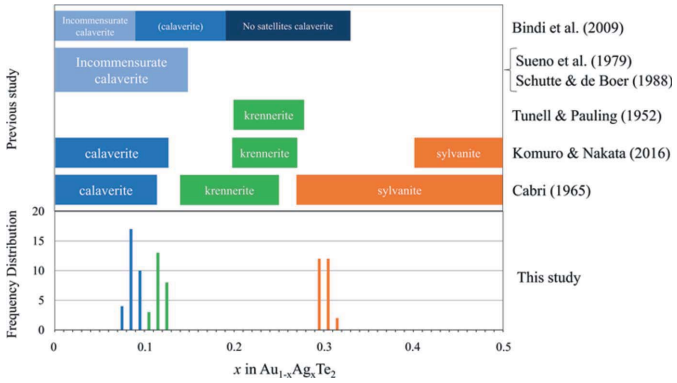

Figure 4
Histogram of analytical values for calaverite, krennerite and sylvanite used in this study, and the range of x values of each mineral having the $Au_{1-x}Ag_xTe_2$ composition reported so far.

4.2. Description of the crystal structure and bonding distances

The crystal structure of the two minerals, krennerite and sylvanite, is hereafter analysed by the Charge Distribution (CHARDI) approach (Hoppe *et al.*, 1989; Nespolo, 2016), the most recent development of Pauling's classical method known as bond strength (Pauling, 1929). CHARDI treats non-molecular crystal structures by approximating each atom by a point charge corresponding to its oxidation number, *i.e.* the same approach used to calculate the Madelung constants (Madelung, 1918). Chemical bonds are assumed to exist only between atoms of opposite charge, *i.e.* between an electropositive and an electronegative atom. The strength of each bond, known as the bond weight (BW), is estimated as a function of the ratio of the experimental bond length and a weighted average of all the bond lengths between the atom centring the coordination polyhedron and the atoms at the corner of it. The weight of each bond decreases exponentially with the bond length; for a uniform polyhedron (a polyhedron in which all centre-to-corner distances are identical), the weighted average distance coincides with the arithmetic mean. The sum of the bond weights gives ECoN, the Effective Coordination Number, which is a real number representing a generalization of the classical concept of coordination number (Hoppe, 1979). The more a coordination polyhedron departs from its ideal shape, the larger is the difference between ECoN and its classical, integer counterpart. The fractional contribution of each chemical bond to ECoN is then used to distribute the charge (oxidation number) of polyhedron-centring among all the atoms at the corners. Summing up this distribution around corner atoms one gets the estimated charge of these atoms; a significant divergence with respect to the input charge (oxidation number) suggests some strain in the structure. Finally, the ratio of the calculated and input charges for the corner atoms are distributed to all the polyhedron-centring atoms; summing up around these atoms gives their estimated charge; a significant divergence with respect to the input charge (oxidation number) means either that the structural model is possibly incorrect, or that the Madelung-type description is unsuitable for that structure, for example because of the presence of chemical bonds between atoms of the same type of charge (both positive or both negative). For details, see Nespolo (2016). Calculations were performed with *CHARDI2015* (Nespolo & Guillot, 2016).

4.2.1. Krennerite. The structure refinement and bond distances (Table 3) are consistent with those proposed by Tunell & Pauling 1952; Pertlik *et al.* (1984*b*) and Dye & Smyth (2012). Pauling ionic radii for Au^+, Ag^+ and Te^{2-} are 1.26, 1.37 and 2.21 Å respectively (Pauling, 1931), whereas covalent

electronic reprint

radii for Au, Ag and Te are 1.36, 1.45 and 1.38 Å, respectively (Cordero *et al.*, 2008). van der Waals radii for Au, Ag and Te are 2.32 Å, 2.53 Å and 1.99 Å, respectively (Alvarez, 2013). The Shannon radii in sulfides are 0.58 Å for $^{II}Au^{+}$, 0.62 Å for $^{IVSQ}Au^{3+}$, 0.71 Å for $^{II}Ag^{+}$, 0.92 Å for $^{IV}Ag^{+}$, and 2.07 Å for $^{VI}Te^{2-}$ (Shannon, 1981).

Krennerite structure has three crystallographically distinct noble metal sites and five distinct Te sites (Table 3). Au1 is on Wyckoff position 2*a*, site-symmetry group ..2, and is occupied by 82.6 (2)% Au and 17.4 (2)% Ag, based on occupancy refinement; it is coordinated by six Te atoms, in a 2+2+2 pattern as originally proposed by Pertlik (1984*b*). The highly distorted configuration is reflected in the ECoN value of 5.18 (for six atoms) and in the significantly lower weighted Au/Ag—Te average distance with respect to the arithmetic mean (2.837 versus 2.913 Å). Au2 is located on Wyckoff position 2*c*, site-symmetry group *m*.., and is occupied by 67.6 (2)% Au and 32.4 (2)% Ag, based on occupancy refinement; it has a similar coordination as Au1; the highly distorted configuration is reflected in the ECoN value of 5.07 (for six atoms) and in the significantly lower weighted average Au/Ag–Te distance, with respect to the arithmetic mean (2.850 versus 2.936 Å). Au3 is on the 4*d* general Wyckoff position and has an almost regular, square planar coordination, with four Au–Te distances concentrated around the average (both arithmetic and weighted) of 2.690 Å, which perfectly coincides with the sum of the Shannon radii; the value of ECoN is 4.00, identical to the classical coordination number. Two further Au–Te distances of 3.3241 (4) and 3.4585 (4) Å are much closer to the sum of Shannon radii for pure ionic (3.47 Å) than for pure covalent (2.74 Å) bonds, which could suggests some ionic contribution to the otherwise strong covalent bond. They however result in negligibly small bond weights, showing that these two contacts can hardly be considered as chemical bonds. On the other hand, a linear coordination of Au1 and Au2 that would be obtained by considering only the strongest covalent bonds, *i.e.* by excluding bonds beyond 2.9 Å, would get rid of contacts whose bond weights (BW) are highly significant (BW = 0.4 to 0.8), resulting in an unsatisfactory description of the structure. This implies that the *sp* hybridization assumed for a linear covalent bond is no longer satisfactory to describe the coordination polyhedra of Au^{+}/Ag^{+}; the distorted rhombic bipyramids can be seen as a deformation of octahedral coordination, for which the hybridization scheme would be by d^2sp^3.

The metal–metal bonds observed in petzite [Au—Ag = 3.0784 (18) Å: Hongu *et al.* 2019*a*], muthmannite [Au—Ag = 3.383 (3) Å: Bindi & Cipriani, 2004] and Ni selenide [Ni—Ni = 2.577 (2) Å: Unoki *et al.*, 2021) are not observed in krennerite. It is evident that the mineral is more closely related to normal salt-like compounds than to intermetallic compounds. The three coordination polyhedra of Au1, Au2 and Au3 sites are linked by Te—Te covalent bonds to crenellated sheets parallel to (010). The $[Te_3]^{2-}$ (Te5—Te1—Te5) and $[Te_2]^{2-}$ (Te3–T4) units are present as well as isolated tellurium atoms (Te2), formally, Te^{2-} ions, bonded only to gold and/or silver atoms (Tunell & Pauling, 1952; Pertlik, 1984*b*). In the $[Te_3]^{2-}$ unit, which occurs also in empressite (Bindi *et al.*, 2004), the central tellurium atom (Te1) is expected to be zerovalent and bonded to two monovalent Te5 atoms, whereas Te2 should be bivalent. These values result in a highly unsatisfactory analysis by CHARDI, which indicate a formal oxidation number of −0.26 for Te1 and −1.72 for Te2, the other tellurium atoms having a charge close to −1. This suggests that, at least within the limits of applicability of a Madelung-type model, the Te1—Te5 bond is not entirely homopolar, which is not surprising knowing that Te5 is bonded to both Au^{3+} and Ag^{+}/Ag^{+}, whereas Te1 only to Ag^{+}/Ag^{+}. Te2 then departs from −2 to keep the electrical neutrality.

There are five distinct Te sites in the structure. The Te1 and Te2 sites have site-symmetry groups of type *m*.., whereas the other Te sites are at general positions. Te1 atom is bonded to two Te5 atoms at 2.8755 (4) Å with bond angle ∠Te5—Te1—Te5 = 96.012 (15)° for the [Te–Te–Te] unit. This value is about 7° smaller than the angle ∠Te—Te—Te = 103.1° in pure Te (Adenis *et al.*, 1989). Te3 atoms is bonded one Te4 at 2.8595 (4) Å for the [Te–Te] unit. Electron sharing can be expected from these short distances, which held together the crenellated sheets [Fig. 1(*d*)]. These sheets are connected into a framework by four crystallographically different Te atoms – combined to one $[Te_3]$ unit (Te5—Te1—Te5) and two $[Te_2]$ unit (Te3–Te4) with Te–Te < 2.9 Å. A fifth isolated Te^{-} (Te2) ion is only surrounded by (Au,Ag) and Au atoms. As Pertlik (1984*b*) suggested, the groups in the Te covalent bonds should be reflected in the chemical formula.

A clear difference appears between krennerite and petzite. Tellurium in petzite is coordinated by one gold atom at 2.6268 (18) Å, and six silver atoms, three at 2.948 Å and three more at 2.9821 (13) Å. Short distances for Ag—Au and Ag—Ag bonds exist in petzite and are very close to the bond distances in metallic gold and silver: 2.88∼2.89 Å (Wyckoff, 1963; Venudhar *et al.*, 1978). There is no Te—Te covalent bond in petzite. On the contrary[In contrast], Te–Te short distances in krennerite (Table 7) indicate the existence of Te—Te bond, whereas no metal–metal bond occurs.

The Au^{+} and Au^{3+} coordination preference and the presence of Te covalent bond units suggests that the structural chemical formula is written as $(Au^{+1}{}_{2-x}Ag^{+1}{}_{x})$-$Au^{+3}{}_{2}[Te_3]^{2-}[Te_2]^{2-}{}_{2}[Te]^{2-}$; x = 0.43–1.12 (our sample, x = 0.43–0.50), in agreement with Pertlik (1984*b*).

4.2.2. Sylvanite. The refined structural model essentially coincides with those proposed earlier by Tunell (1941) and Pertlik (1984*a*). Previous researchers described the structure as Au occupying a distorted $AuTe_6$ octahedral site. The $AgTe_6$ polyhedra forms sheets by sharing edges parallel to (100) of *P*2/*c* setting, *i.e.* (200) of *B*2/*e* setting (Nespolo, 2015). Kostovite, $CuAuTe_2Ca_{1-x}Au_{1+x}Te_4$, is closely related to sylvanite (Van Tendeloo & Amelinckx, 1986).

Au1 site is fully occupied by Au^{3+}; it is on 4*a* Wyckoff position, site-symmetry group 1, in square planar coordination. ECoN is 3.99 and the equality of weighted average and arithmetic mean Au–Te distance (2.683 Å) shows that the polyhedron is close to uniform. The [4+2] coordination proposed by Pertlik (1984*a*) cannot be retained, because the

electronic reprint

longer Au1–Te2 contacts of 3.3294 (6) Å result in a negligible bond weight (0.085).

Au2 site occupancy refined to 0.3609 (19) Au and 0.6391 (19) A g. It is on 4*e* Wyckoff position, with site-symmetry group 2. It is coordinated by six Te atoms, in a 2+2+2 pattern. The configuration is highly distorted, as reflected by the ECoN value of 4.98 (for six atoms) and by the significantly lower weighted average Au/Ag–Te distance, with respect to the arithmetic mean (2.862 versus 2.962 Å).

The Charge Distribution analysis is perfectly satisfactory, showing that a Madelung-type model based on $Au1^{3+}Te^{-}_{4}$ and $(Au^{+}Ag^{+})Te^{-}_{6}$ polyhedra correctly describes the structure, despite the fact that, similarly to krennerite, the 'sheets' are linked to form a network by [Te_2] unit with Te1–Te2 distance of 2.8281 (19) Å [Fig. 1(*b*)]. The fact that a Madelung-type description is satisfactory for sylvanite while it is not for krennerite suggests that the role of the Te—Te bonding is more fundamental for the latter than for the former; as shown in the following section, its covalent character is more pronounced in krennerite. The Au^{+} and Au^{3+} coordination preference and the presence of Te—Te covalent bond units suggests that the crystal chemical formula can be written as $Au^{3+}(Au^{+}_{1-x}Ag^{+}_{x})[Te_2]^{2-}_{2}$; x = 0.27–0.50 (our sample, x = 0.29–0.31) This also well expresses the charge balance and the characteristic of Au^{+} and Au^{3+}, with electric configurations $5d^{10}$ and $5d^{8}$, respectively.

In sylvanite, one tellurium atom (Te1) binds tightly to three Au/Ag atoms and to the other tellurium (Te2). It is located close to an edge of an irregular disphenoid (Fig. 5), which is highly different from the digonal tetrahedron in the pyrite-type compound. The coordination environments around the Sb—Sb covalent bond in pyrite-type aurostibite $AuSb_2$ (Graham & Kaiman, 1952) and the Te—Te covalent bond in sylvanite are compared in Fig. 6, where strong Au—Sb, Sb—Sb, Au—Te and Te—Te bonds are shown. In $AuSb_2$, the Sb—Sb covalent bond is located at a threefold rotoinversion axis, and the polyhedron around Sb–Sb is a trigonal antiprism. On the other hand, the polyhedron around Te–Te in sylvanite is distorted, and the three ∠Te—Te—(Au, Ag) angles are 96.25 (3)°, 103.25 (3)° and 158.643 (11)°. The two shortest Te2–Te1 contacts are 2.8281 (11) Å (edge of the irregular disphenoid) and 3.5796 (13), which is significantly shorter than the sum of van der Waals radii for Te, 3.98 Å (Alvarez, 2013). Such a chalcogen–chalcogen intermediate distances do not appear in pyrite-type compounds. and may play a role in the formation of sylvanite.

4.2.3. Au L_{III}-edge and Te *K*-edge XANES spectra and bonding nature of Au and Te. Fig. 7 shows the Au L_{III}-edge and Te *K*-edge XANES spectra for calaverite, krennerite, sylvanite and reference materials. It was observed that the threshold energies of these materials ranged from 11.9167 keV to 11.9186 keV, with a difference of only 1.9 eV. The XANES patterns of gold and of period V and VI elements in compounds vary depending on the chemical bonding state and structure (Hongu *et al.*, 2019*a*,*b*; Yoshiasa *et al.*, 2019). Clear differences in peak shape have been observed in gold minerals such as petzite, aurostibite ($AuSb_2$) and nagyagite (Hongu *et al.*, 2019*a*). The patterns of the Au L_{III}-edge and Te *K*-edge XANES spectra are very similar for calaverite, krennerite and sylvanite. The results indicate that the local structures of these three minerals are almost the same. On the high-energy side of

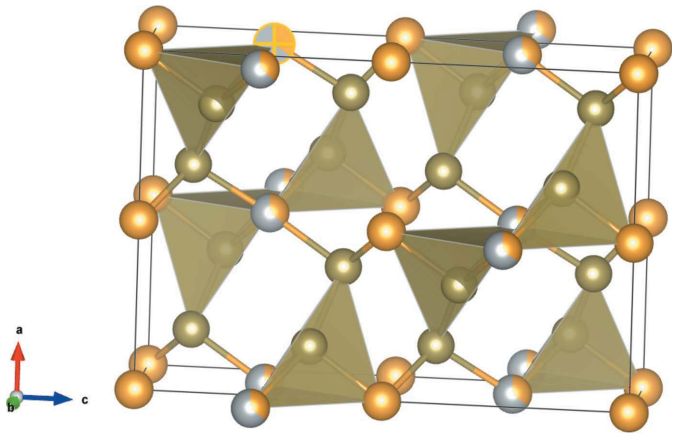

Figure 5
The structure of sylvanite described as anion-centred, to emphasize the coordination around Te1.

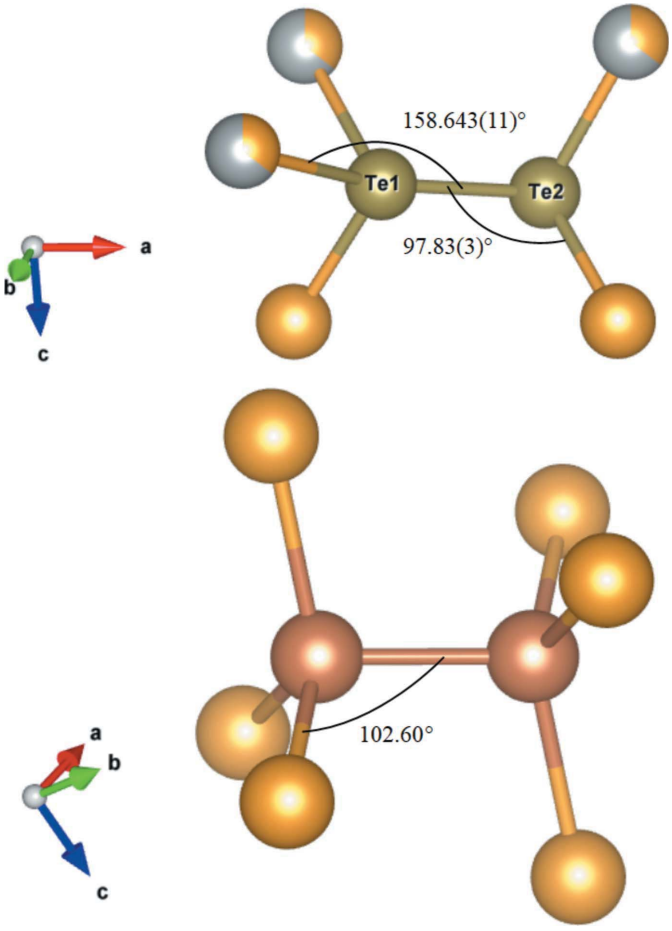

Figure 6
Comparison of the coordination environments around the Te—Te covalent bond in sylvanite and the Sb—Sb covalent bond in pyrite-type AuSb2, where strong Au—Sb, Sb—Sb, Au—Te and Te—Te bonds are shown.

electronic reprint

the absorption edge in Au L_{III}-edge XANES spectrum for these materials in Fig. 7, a first peak (white line) appears due to electron transfer from gold to tellurium. The degree of electron transfer in calaverite, krennerite and sylvanite is intermediate between the insulator $AuBr_3$ or AuCl and the electron conductor Au metal. These aspects differ from the results of spectroscopy with surface-sensitive soft X-rays [van Triest *et al.* (1990) and Ettema *et al.* (1994)]. The expected abundance ratio of Au^+ to Au^{3+} in calaverite (Au^+: Au^{3+} = 0.83: 1.0) and in krennerite (Au^+: Au^{3+} = 0.76: 1.0) is lower than that in sylvanite (Au^+: Au^{3+} = 0.39: 1.0) estimated from the compositions in Table 1. The threshold energy of Au L_{III}-edge XANES spectrum for sylvanite [11.9182 (1) keV] shifts 0.5 eV to the higher energy side with respect to those for calaverite [11.9177 (1) keV] and krennerite [11.9177 (1) keV]. Because of the large number of electrons in gold, the chemical shift of the threshold energy resulting from the difference between the monovalent and trivalent states is limited. Mössbauer data (Wagner *et al.*, 1994) confirmed the notion that the square-planar coordinated sites contain Au^{3+} with a moderate degree of bond covalency and that the nearest-neighbour environment of the gold atoms on 2+2+2 sites is very similar in sylvanite, krennerite and calaverite showing the covalent coordination for Au^+. The results of our XANES experiment are therefore in agreement with the results of Mössbauer data.

The threshold energy of Te *K*-edge XANES spectrum for krennerite [31.7587 (1) keV] shifts 1.9 eV to the higher energy side with respect to those for calaverite [31.7568 (1) keV] and sylvanite [31.7568 (1) keV]. The chemical bonding of Te in krennerite has a more covalent character than that in calaverite and sylvanite. The presence of $[Te_3]^{2-}$ unit seems to influence the chemical shift. The shape of both Au L_{III}-edge and Te *K*-edge XANES spectra for calaverite clearly matches that of sylvanite. This means that the local structure and chemical bonding state of gold and tellurium in calaverite and sylvanite are the same within the current resolution.

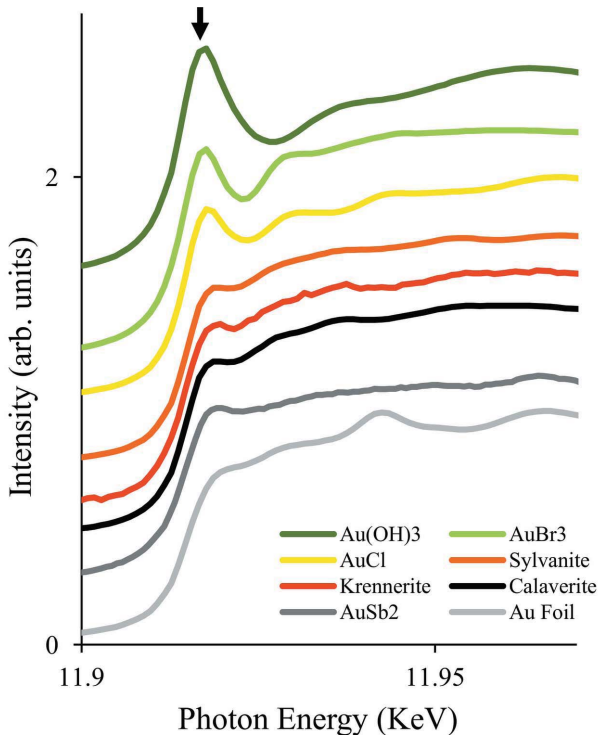

Figure 7
Au L_{III}-edge and Te *K*-edge XANES spectra for calaverite, krennerite, sylvanite and reference Au materials. The arrow indicates the white line at the absorption edges.

4.3. Comparison of Debye temperatures obtained from the Debye–Waller factor

The Debye–Waller factors obtained from diffraction experiments include the effects of static and dynamic disorders. The static disorder is the configurational disorder, while the dynamic disorder arises from the thermal vibration of atoms. The Debye temperature θ_D for each atom can be estimated using the dynamic part in Debye–Waller factor based on the Debye approximation (Willis & Pryor, 1975; Wood *et al.*, 2002; Christensen *et al.*, 2006; Nakatsuka *et al.*, 2011; Yoshiasa *et al.*, 2016, 2021). We have estimated θ_D for each atom in sites occupied solely by Au or Te using the values of U_{eq} (Tables 3 and 5) under the assumption of no configurational disorder of atoms (the site where Ag substitutes for Au does contain configurational disorder components). Obtained θ_D values for Au in the Au3 site, Te in the Te2 and Te4 sites in krennerite are 126 K, 162 K and 154 K, respectively. The θ_D values for Au in the Au1 site, Te in the T1 and Te2 sites in sylvanite are 125 K, 151 K and 155 K, respectively. The Debye temperatures are directly related to the melting temperature, the formation temperature and the occurrence of minerals. Those for Au sites occupied by 100% Au in krennerite (126 K) and sylvanite (125 K) are significantly lower than the corresponding θ_D value of 178 K for the pure gold metals. The Debye temperature for the site with the highest value in the crystal corresponds to the bulk Debye temperature of the compound (Tokuda *et al.*, 2019; Yoshiasa *et al.*, 2021). The Debye temperatures of Te atoms are responsible for bulk θ_D in these minerals. The bulk θ_D of krennerite and sylvanite are 162 K and 155 K, respectively. These bulk θ_D values for krennerite and sylvanite are close to 158 K for pure tellurium with a covalent structure. The melting points of 464–400°C for these minerals (Cabri, 1965) are close to the value of 452.5°C for pure tellurium. The Debye temperatures of these minerals are compared with the melting points of 464°C for AuTe2 (Tunell & Pauling, 1952).

In krennerite and sylvanite, there is no site that shows any unusual value of the Debye–Waller factor, such as U_{22} = 0.100 (3) Å ^{2} of the Te site in pure calaverite (Reithmayer *et al.*, 1993). The values of U_{22} (Te) and U_{eq} ($Au_{0.86}Ag_{0.14}$) are also 0.113 (2) $Å^2$ and 0.013 (2) $Å^2$, respectively, in the average structural analysis of calaverite at 298 K by Schutte & de Boer (1988). In addition to the dynamic vibrational effect, the configurational effect by incommensurate modulation is included in the unusual value observed only at U_{22} (Te) of 0.113 (2) $Å^2$. That is, the unusual value is mainly due to a configurational disorder that reflects the modulation distur-

electronic reprint

bance. On the other hands, the values of U_{eq} of 0.0132 (8) Å^2 for Au by (Reithmayer *et al.*, 1993) and U_{eq} of 0.013 (2) Å^2 for ($Au_{0.86}Ag_{0.14}$) by Schutte & de Boer (1988) in calaverite are normal, not an unusual value, compared to those of U_{eq} for Au3 in krennerite and U_{eq} for Au1 in sylvanite (Tables 4 and 6). The Debye–Waller factor U_{eq} of Au site in calaverite may be considered to have little static effect. Debye temperature θ_D of Au in pure calaverite was estimated to be 128 K under the assumption of no configurational disorder components. The θ_D of 128 K in calaverite was almost the same value as krennerite and sylvanite, and is a slightly higher than the temperature of 120 K for krennerite and 121 K for sylvanite. It may correspond to the observation by Cabri (1965) that the melting point of calaverite is slightly higher than those of krennerite and sylvanite.

4.4. Au—Te and Te—Te bonds in calaverite, krennerite and sylvanite

Fig. 8 shows the relationship between the Au content in each noble metal site and the (Au,Ag)–Te distance in some gold and silver tellurides, from which a clear trend between the Au content and the bond distance appears. Localized covalent, strong and weak electrostatic interactions coexist as three bonding states. The shortest covalent bond distance is about 2.69 (krennerite)–2.72 (sylvanite) Å for Au^+–Te in the highly distorted 2+2+2 coordination, 2.67 Å for $^{IV}Au^{3+}$–Te, and 2.77 Å for probably $^{VI}Au^{2+}$–Te (under high pressure), respectively. Similar to the structure analyses proposed in the past by Pertlik *et al.* (1984*a*,*b*) and Dye & Smyth (2012), our results for krennerite and sylvanite confirm the existence of a site occupied by Au alone. CHARDI confirms that the Au3 site in krennerite and the Au1 site in sylvanite are both occupied by Au^{3+}, in square planar coordination. Krennerite and sylvanite have other sites where gold is partially substituted by silver. The difference between the shortest covalent bond distances of the highly distorted 2+2+2 coordinated (Au,Ag)$^+$–Te and 4-coordinated Au^{3+}–Te in krennerite and sylvanite is about 0.02 Å. The monovalent cations, whose ionic radius is larger than those of the trivalent metal state, have similar shortest bond distances but span a much larger interval, due to their highly distorted coordination. The key to complex but regularly arranged structure formation for krennerite and sylvanite is that Ag^+ can reliably form a 2+2+2 covalent coordination. This indicates the importance of the presence of Ag^+. CHARDI confirms that gold occurs as monovalent in these sites.

In Fig. 9, the Te–Te distances in calaverite (average structure model at ambient conditions by Reithmayer *et al.*, 1993), krennerite and sylvanite were plotted against x in $Au_{1-x}Ag_xTe_2$. The Te–Te distances of 2.81–2.88 Å in Fig. 9 indicate the existence of strong covalent bonds between tellurium atoms. Short Te–Te contacts were pointed out by Shutte & de Boer (1988) and Streltsov *et al.* (2018). The Te–Te distances of 3.40–3.97 Å, shorter than the van der Waals bonding distance of 3.98 Å for Te–Te, suggest a weak interaction between tellurium atoms. While systematic trends of Te–Te are observed, the Te–Te distance of 3.2 Å in calaverite departs from the trend and represents an unusual value with respect to the typical Te–Te distances in various samples. The usual Te—Te covalent bonds (*i.e.* < 2.9 Å) that occur in the krennerite and sylvanite are not observed in the average structure of calaverite. This should be a clue to the solution of the occurrence of the incommensurate structure.

Tunell & Ksanda (1936) and Tunell & Pauling (1952) solved the average *C*2/*m* structure of calaverite. The average structure has one noble metal site and one Te site. Au and Te sites have site-symmetry groups of type 2/*m* and of *m*, respectively. The average structure of calaverite has been described as a distorted CdI_2-type structure. In calaverite, the noble metal atoms are surrounded by distorted octahedra of Te atoms with two Au–Te distances of 2.67 Å and four of 2.98 Å [Fig. 1(*a*)].

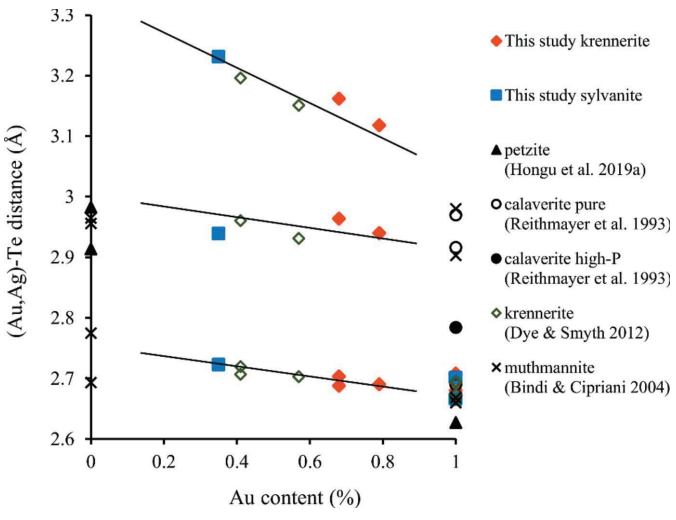

Figure 8
Relationship between the Au content in each noble metal site and the (Au,Ag)–Te distance in gold and silver tellurides.

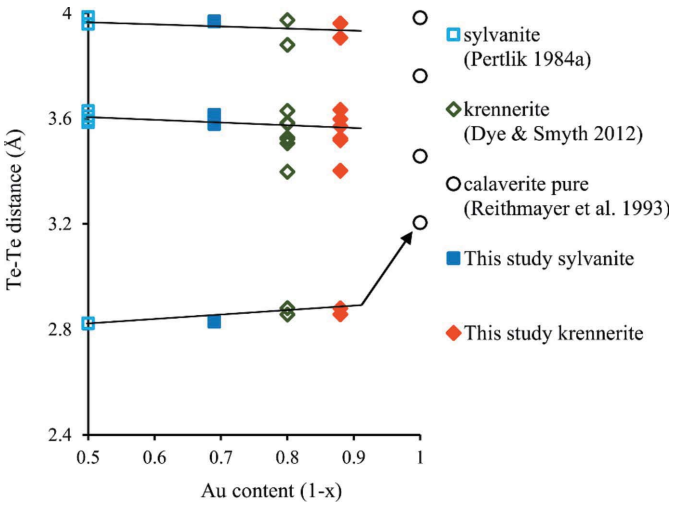

Figure 9
The Te–Te distances in calaverite (average structure model at ambient conditions by Reithmayer *et al.* 1993), krennerite [Dye & Smyth (2012) and this study] and sylvanite [Pertlik (1984*a*) and this study] were plotted against x in $Au_{1-x}Ag_xTe_2$.

electronic reprint

Au^{+} forms a 2+2+2 coordination covalent bond, but Au^{3+} does not. The van der Waals bond length of Te—Te is 3.98 Å. Each Te atom is surrounded by three metal atoms and five Te atoms; it is equally close to two of its five Te neighbours at 3.20 Å, with the third Te neighbour at 3.45 Å and the last two at an even greater distance of 3.77 Å (Fig. 9). As shown in Section 2, calaverite and sylvanite have very closely related crystal structures (Fig. 2). However, the Te–Te shortest distances connecting the octahedral layers is 3.20 Å in the average structure of calaverite but only 2.8281 (19) Å in sylvanite.

As we discussed before, the effect of configurational disorder in Debye–Waller factors for Au in pure calaverite should be negligible, the dynamic effects being predominant. Fig. 10 shows the displacement ellipsoid in the calaverite structure based on the data of the average structure analysis of Schutte & de Boer (1988). The extension of Debye–Waller factor U_{22} for Te along the *b*-axis direction is clear. Only Te (U_{22} in the Te site) shows the effect of statistical arrangement of one-dimensional modulation. The root mean square displacement of U_{22} in calaverite reaches an amplitude of 0.32 Å. The split-atom positions (atomic coordinates 0.688, 0.070, 0.288) away from the centre of the Te site (0.688, 0.0, 0.288) on a mirror plane is indicated by red spheres in Fig. 10. The distance between the centre of Te site and the split atom position is 0.31 Å. The position of the red spheres corresponds well to the split atom position presented by Sueno *et al.* (1979), who have shown on the differential Fourier map that the Te atom position is split from its supposed position on the mirror plane in a symmetrical dumbbell shape distribution. The distance between the two peaks of the electron cloud of Te atom was about 0.5 Å. According to Bindi *et al.* (2009) (Table 8 therein) the amplitude of the (Au,Ag) positional modulation was zero within one standard deviation, and that for Te positional modulation was very large in the *b*-axis direction. In Schutte and de Boer (1988) (Table 6 therein), the term of $\sin(2\pi - x^4)$ for the *y*-coordinate of Te was also analysed as the main factor of modulation; that is, it was shown that the cause of modulation is mainly the displacement of Te along in *b*-axis. In the average structure this is reflected in the unusual Debye–Waller factor U_{22} of Te, which extends perpendicular to the one-dimensional modulation vector and also perpendicular to the Au—Te short covalent bond.

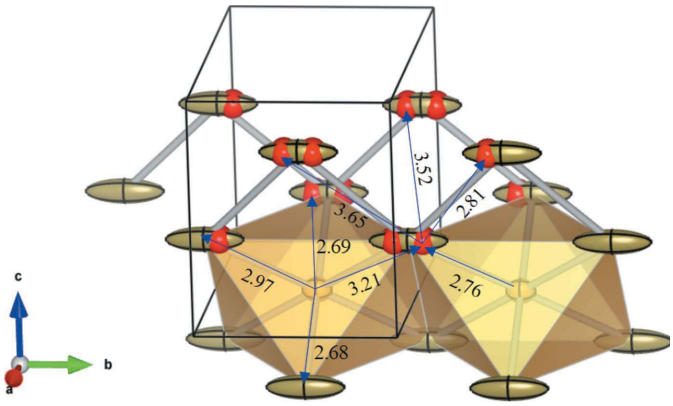

Figure 10
Displacement ellipsoids in the calaverite structure based on the data of the average structure analysis of Schutte & De Boer (1988). The split atom positions ($y = 0.070$) away from the centre of the Te site ($y = 0$) on a mirror plane is indicated by red spheres. Distances are given in Å.

The Au–Te (2.67, 2.68, 2.69, 2.70, 2.93, 2.96 and 3.15 Å) and Te–Te (2.83, 3.59 and 3.601 Å) distances found in sylvanite have much in common with the distances around the position of the red spheres in Fig. 10. In other words, the distances required for sylvanite-like structure formation, such as the square planar covalent Au–Te distances for Au^{3+}, strong electrostatic interaction distances and strong covalent Te–Te distances, can be derived only from the static displacement of Te along the *b*-axis direction, in addition to linear covalent Au–Te distance (Fig. 7). The elongated MSD of Te in calaverite should be mainly caused by the configurational disorder of the $[Te_2]^{2-}$ unit, which form both the 2+2+2 coordinated Au^{+} and square planar coordinated Au^{3+} ions arrangement. Because the interatomic distances and the shape of Au L_{III}- and Te *K*-edge XANES spectra for calaverite and sylvanite have common characteristics, we propose the chemical formula for calaverite as $(Au_{1-x}Ag_x)^{+}\ Au^{3+}\ [Te_2]^{2-}{}_2$, which corresponds to the formula proposed by Pertlik (1984*c*).

4.5. Split-atom positions of Te and incommensurate modulation in calaverite

Schutte & de Boer (1988) solved the incommensurately modulated structure of calaverite using the superspace approach in a superspace group of type $C2/m(\alpha 0\gamma)0s$. The authors showed that the modulation consists mainly of displacement of Te atoms and interpreted the observed modulations in terms of valence fluctuations between Au^{+} and Au^{3+}. The metal–tellurium distances have been represented in their figures as a function of the phase of the modulation wave. Note that the results by Bindi *et al.* (2009) seem to suggest a discontinuous modulation of Te atoms, contrary Schutte & de Boer (1988), who reported that two Te atoms at linear coordinated Au–Te distances of 2.67 Å were hardly modulated. However, the distances of 2.98 Å for the other four Au–Te were strongly modulated. The coordination of the noble metal atoms by Te is modified by the modulation. Two- and four-coordination of metal sites with a distance of about 2.68 Å appear repeatedly as a function of the phase of the modulation wave. Their analyses showed that the large displacements of the Te atoms modifies the coordination of the metal atom from linear to square and that the modulation of calaverite is caused by a fluctuation of the coordination environments around Au atoms, between Au^{+} with a linear coordination of Te, and Au^{3+} with a square planar coordination. This valence fluctuation induces mainly the strong modulations of the Te position in calaverite structure (Schutte & de Boer, 1988; Bindi *et al.*, 2009). Our interpretation of the distances shown in Fig. 7 by comparison with sylvanite is in good agreement with the analyses of the incommensurately modulated structures of calaverite by Schutte & de Boer (1988).

electronic reprint

Analyses of the incommensurately modulated structures were also performed in a superspace group of the same type for calaverite with x = 0.0–0.09 in $Au_{1-x}Ag_xTe_2$ by Bindi *et al.* (2009). They presented the variation of Au–Te distances as a function of the phase of the modulation wave, which is quite different from those by Schutte & de Boer (1988). In Bindi *et al.* (2009), the change in distance of 2.98 Å is small and the square planar coordinated Au does not appear. No satellite peaks were observed in calaverite with compositions of x = 0.19 and x = 0.33. Pertlik (1984*c*) analysed calaverite using an acentric space group of type *Pc* and showed the existence of the square planar coordinated Au and the $[Te_2]$ unit. Calaverite may have various average structures depending on the formation conditions.

Sueno *et al.* (1979) suggested that the modulation of the structure of calaverite is mainly due to the displacement of Te along only one direction, with almost no displacement of Au and Ag atoms. Disturbance in only one direction is the key feature of elucidating the reason for the appearance of the incommensurate modulation.

Schutte & de Boer (1988) represented a continuous variation from a linear to a square-planar coordination in calaverite as a function of the modulation. At the same time, the Te–Te distances of 2.81 Å for $[Te_2]$ unit and its pair, 3.61 Å, appeared in their analyses as the main distances. These Te–Te distances correspond well with the 2.80 Å and 3.64 Å shown in our Fig. 7. A number of charge-balanced local structures, such as $Au^{3+}Au^{+}{}_3[Te_3]^{2-}{}_2[Te_2]^{2-}$, $Au^{3+}Au^{+}[Te_2]^{2-}{}_2$ and $Au^{3+}Au^{+}[Te_3]^{2-}Te^{2-}$, $Au^{3+}{}_2[Te_2]^{2-}Te^{2-}{}_2$, can be constructed from the valence fluctuation of Au and the variety of covalent bond units of Te. The average composition is stoichiometric $(Au,Ag)Te_2$ as confirmed by chemical analyses. The covalently bonded $[Te_3]^{2-}$ and $[Te_2]^{2-}$ units and Te^{2-} telluride ion found in krennerite should exist in calaverite as well. The structure of calaverite is close to that of sylvanite than to that of krennerite, and the $[Te_3]^{2-}$ unit and the Te^{2-} ion should not be the main components. The noble metal is located at the centre of a particular crystal site of calaverite, and the position itself does not cause configurational disorder. Since the periodicity of atomic arrangement reduces the energy of the crystal, the material tends toward a crystal structure that is as periodic as possible. Calaverite does not take structures with more complicated fluctuations. An important factor in the formation of the incommensurate modulation in which the satellite diffractions appear only along one direction is that a stable local structure can be formed by shifting the Te atoms only along the *b*-axis direction.

4.6. Important role of Ag in krennerite and sylvanite

Since Tunell & Pauling (1952), it has been described that the structures of krennerite and sylvanite are built on a modified calaverite structure. Van Tendeloo *et al.* (1984) considered krennerite as a twin-interface-modulated long-period superstructure of calaverite. Van Tendeloo *et al.* (1983) stated the mineral sylvanite as a commensurately modulated superstructure of calaverite. In §2 we have shown the close similarity between the structure of sylvanite and the calaverite prototype. Compared to sylvanite, the crystallization of krennerite requires the formation of $[Te_3]^{2-}$ unit and the presence of Te^{2-} ions, as well as their regular arrangement. In addition, Ag^{+} ions occupy two different kinds of sites. Krennerite is a low symmetry stable phase in which atoms are regularly arranged with charge balance maintained by the appearance of diversity in Te—Te covalent units and bond lengths.

Schutte & de Boer (1988) suggested that an ordered distribution of Ag induces very strong valence fluctuation of Au in the structure, and that the occupation modulation in the (Au, Ag) position strengthens the coordination differentiation. Bindi *et al.* (2009) claimed that the ordered distribution of silver reinforces the valence fluctuation of Au. However, regular structures occur in the composition range with higher Ag contents, covering the composition of calaverite, krennerite and sylvanite solid-solutions (Fig. 4). A non-modulated crystal structure therefore occurs when a certain amount of Ag^{+} is added. Since Ag ion takes a 2+2+2 covalent coordination in these minerals, it has the effect of suppressing fluctuations and increasing regularity. It clearly appears that Ag^{+} promotes three-dimensional periodicity in krennerite and sylvanite.

The structure of calaverite with usual regular arrangement is not formed under ambient conditions. Three-dimensional periodicity of pure $AuTe_2$ calaverite crystal is disturbed in the absence of pressure (Reithmayer *et al.*, 1993). The formation of various kinds of Te covalent units ($[Te_3]$, $[Te_2]$ and Te^{2-}) contributes to the stability of the krennerite and sylvanite, and to formation of local structure without the incommensurate modulation that occurs instead in calaverite, where such units are absent. These various Te—Te covalent units appear to prevent the occurrence of modulation. A few local structures like krennerite may be formed in the modulated calaverite structure, but the main structure will be formed with a local structure similar to that of sylvanite.

In the Ag-poor region corresponding to calaverite almost no rearrangement of Te occurred even when the temperature was raised (Sueno *et al.*, 1979; Schutte & de Boer, 1988). The inability to adopt a regular triperiodic arrangement like that of krennerite and sylvanite, resulting in the modulation observed unless pressure is raised, is probably related to the ambiguity between Au^{+} and Au^{3+} during crystal growth. Streltsov *et al.* (2018) showed theoretically that $AuAu'Te_4$ (Au-end-member) with sylvanite structure is stable and the structure is lower in energy than the average $C2/m$ structure. The stoichiometry requires an equal amount of Au^{+}:Au^{3+} on average, but local fluctuations may and probably do occur. As we have seen, the coordination of gold in the two valence states is not the same: Au^{3+} prefers a slightly distorted square planar coordination corresponding to dsp^2 hybridization, whereas Au^{+} occurs in the 2+2+2 coordination of a distorted rhombic bipyramid corresponding to d^2sp^3 hybridization. During crystal growth, local structures differing from the average structure may occur; rearrangements to fit the triperiodic distribution of Au^{3+} and Au^{+} corresponding to the average structure may

electronic reprint

occur by electron hopping, a process that does not require rearrangement of atoms. This would however result in an unfavourable coordination for the new valence state, which may generate local strains possibly resulting in small displacements of the metal atoms to approach their natural coordination. These displacements may be the reason for the occurrence of modulation in calaverite.

Summarizing, two points seem to play a role in the formation of the incommensurate modulation. First, various local structures can be created by shifting Te atom along the *b*-axis direction. Second, the ambiguity in the formation of valence state of gold ions between monovalent and trivalent during crystal growth accompanied by electron transfer to Te atoms.

In kostovite, where Ag is replaced by Cu, the solid solution between Cu and Au will be probably more restricted. In fact, Bonev *et al.* (2005) revealed the existence in Nature of a miscibility gap between sylvanite and Ag-rich kostovite.

5. Conclusions

The absence of incommensurate modulation in sylvanite and krennerite seems to be related to the presence of Ag^{+} and relatively strong Te—Te bonds (< 2.9 Å), whereas strong and weak Te—Te bonds appear in the modulated structure of calaverite, due to the configurational disorder; the modulation may be related to the ambiguity between Au^{+} and Au^{3+} during crystal growth. Electron hopping during crystal growth transforming Au^{+} into Au^{3+} or vice versa, results in an unfavourable coordination for the new valence state; the local strain it generates may lead to small displacements of the metal atoms to approach their natural coordination. Our results support the theoretical considerations by Streltsov *et al.* (2018), suggesting that sylvanite structure is stable and has lower energy than the *C*2/*m* average calaverite structure.

Acknowledgements

Critical comments from Dr Yves Moëlo (Université de Nantes) and an anonymous reviewer are gratefully acknowledged.

Funding information

This research was partially supported by JST SPRING grant number JPMJSP2127 and JSPS KAKENHI grant number JP20H00189.

References

Adenis, C., Langer, V. & Lindqvist, O. (1989). *Acta Cryst.* C**45**, 941–942.
Alvarez, S. (2013). *Dalton Trans.* **42**, 8617–8636.
Bachechi, F. (1971). *Nat. Phys. Sci.* **231**, 67–68.
Bindi, L., Arakcheeva, A. & Chapuis, G. (2009). *Am. Mineral.* **94**, 728–736.
Bindi, L. & Cipriani, C. (2004). *Am. Mineral.* **89**, 1505–1509.
Bindi, L. & Keutsch, F. N. (2018). *Z. Kristallogr.* **233**, 247–253.
Bindi, L., Rossell, M. D., Van Tendeloo, G., Spry, P. G. & Cipriani, C. (2005). *Mineral. Petrol.* **83**, 283–293.
Bindi, L., Spry, P. G. & Cipriani, C. (2004). *Am. Mineral.* **89**, 1043–1047.
Bonev, I. K., Petrunov, R., Cook, N. J. & Ciobanu, C. L. (2005). *Bulg. Acad. Sci. Geochem. Mineral. Petrol.* **42**, 1–22.
Busing, W. R. & Levy, H. A. (1957). *Acta Cryst.* **10**, 180–182.
Cabri, L. J. (1965). *Econ. Geol.* **60**, 1569–1606.
Christensen, M., Lock, N., Overgaard, J. & Iversen, B. B. (2006). *J. Am. Chem. Soc.* **128**, 15657–15665.
Cordero, B., Gómez, V., Platero-Prats, A. E., Revés, M., Echeverría, J., Cremades, E., Barragán, F. & Alvarez, S. (2008). *Dalton Trans.* pp. 2832–2838.
Cotton, F. A. & Wilkinson, G. (1980). *Advance Inorganic Chemistry*, 4th ed., p. 647. New York: John Wiley & Sons.
Dye, M. D. & Smyth, J. R. (2012). *Can. Mineral.* **50**, 119–127.
Elliott, N. & Pauling, L. (1938). *J. Am. Chem. Soc.* **60**, 1846–1851.
Ettema, A. R. H. F., Stegink, T. A. & Haas, C. (1994). *Solid State Commun.* **90**, 211–213.
Ewald, P. P. & Friedrich, W. (1914). *Ann. Phys.* **349**, 1183–1196.
Graham, A. R. & Kaiman, S. (1952). *Am. Mineral.* **37**, 461–469.
Hongu, H., Yoshiasa, A., Nespolo, M., Tobase, T., Tokuda, M. & Sugiyama, K. (2019*a*). *Acta Cryst.* B**75**, 273–278.
Hongu, H., Yoshiasa, A., Tobase, T., Okube, M., Sugiyama, K. & Sato, T. (2019*b*). *Mineral. Petrological Sci.* **114**, 224–230.
Hoppe, R. (1979). *Z. Kristallogr.* **150**, 23–52.
Hoppe, R., Voigt, S., Glaum, H., Kissel, J., Müller, H. P. & Bernet, K. (1989). *J. Less-Common Met.* **156**, 105–122.
Hu, Z. & Gao, S. (2008). *Chem. Geol.* **253**, 205–221.
Janner, A. & Dam, B. (1989). *Acta Cryst.* A**45**, 115–123.
Kitagawa, S., Kotegawa, H., Tou, H., Ishii, H., Kudo, K., Nohara, M. & Harima, H. (2013). *J. Phys. Soc. Jpn*, **82**, 113704.
Komuro, K. & Nakata, M. (2016). *Resour. Geol.* **67**, 22–34.
Madelung, E. (1918). *Phys. Z.* **19**, 524–533.
Momma, K. & Izumi, F. (2011). *J. Appl. Cryst.* **44**, 1272–1276.
Nakatsuka, A., Shimokawa, M., Nakayama, N., Ohtaka, O., Arima, H., Okube, M. & Yoshiasa, A. (2011). *Am. Mineral.* **96**, 1593–1605.
Nespolo, M. (2015). *J. Appl. Cryst.* **48**, 1290–1298.
Nespolo, M. (2016). *Acta Cryst.* B**72**, 51–66.
Nespolo, M. & Aroyo, M. I. (2016). *Acta Cryst.* A**72**, 523–538.
Nespolo, M. & Guillot, B. (2016). *J. Appl. Cryst.* **49**, 317–321.
Pauling, L. (1929). *J. Am. Chem. Soc.* **51**, 1010–1026.
Pauling, L. (1931). *J. Am. Chem. Soc.* **53**, 1367–1400.
Pertlik, F. (1984*a*). *TMPM Tschermaks Mineral. Petrogr. Mitt.* **33**, 203–212.
Pertlik, F. (1984*b*). *TMPM Tschermaks Mineral. Petrogr. Mitt.* **33**, 253–262.
Pertlik, F. (1984*c*). *Z. Kristallogr. Cryst. Mater.* **169**, 227–236.
Petříček, V., Dušek, M. & Palatinus, L. (2014). *Z. Kristallogr.* **229**, 345–352.
Preiß, S., Förster, C., Otto, S., Bauer, M., Müller, P., Hinderberger, D., Hashemi Haeri, H., Carella, L. & Heinze, K. (2017). *Nat. Chem.* **9**, 1249–1255.
Reithmayer, K., Steurer, W., Schulz, H. & de Boer, J. L. (1993). *Acta Cryst.* B**49**, 6–11.
Rigaku OD (2017). *CrysAlis PRO*. Rigaku Oxford Diffraction Ltd, Yarnton, Oxfordshire, England.
Schneider, J. & Schulz, H. (1993). *Z. Kristallogr.* **203**, 1–15.
Schutte, W. J. & de Boer, J. L. (1988). *Acta Cryst.* B**44**, 486–494.
Shannon, R. D. (1981). *Structure and Bonding in Crystals*, Vol. **2**, pp. 53–70.
Streltsov, S. V., Roizen, V. V., Ushakov, A. V., Oganov, A. R. & Khomskii, D. I. (2018). *PNAS*, **115**, 9945–9950.
Sueno, S., Kimata, M. & Ohmasa, M. (1979). *AIP Conf. Proc.* pp. 333–335.
Thompson, R. M. (1949). *Am. Mineral.* **34**, 341–382.
Tobase, T., Yoshiasa, A., Hiratoko, T. & Nakatsuka, A. (2018). *J. Synchrotron Rad.* **25**, 1129–1134.

electronic reprint

Tokuda, M., Yoshiasa, A., Mashimo, T., Arima, H., Hongu, H., Tobase, T., Nakatsuka, A. & Sugiyama, K. (2019). *Z. Kristallogr. Cryst. Mater.* **234**, 371–377.
Triest, A. van, Folkerts, W. & Haas, C. (1990). *J. Phys. Condens. Matter*, **2**, 8733–8740.
Tunell, G. (1941). *Am. Mineral.* **26**, 457–477.
Tunell, G. & Ksanda, C. J. (1936). *J. Wash. Acad. Sci.* **26**, 507–509.
Tunell, G. & Murata, J. (1950). *Am. Mineral.* **35**, 959–984.
Tunell, G. & Pauling, L. (1952). *Acta Cryst.* **5**, 375–381.
Unoki, K., Yoshiasa, A., Kitahara, G., Nishiayama, T., Tokuda, M., Sugiyama, K. & Nakatsuka, A. (2021). *Acta Cryst.* C**77**, 169–175.
Van Tendeloo, G. & Amelinckx, S. (1986). *Acta Cryst.* B**42**, 121–130.
Van Tendeloo, G., Amelinckx, S. & Gregoriades, P. (1984). *J. Solid State Chem.* **53**, 281–289.
Van Tendeloo, G., Gregoriades, P. & Amelinckx, S. (1983). *J. Solid State Chem.* **50**, 335–361.
Venudhar, Y. C., Iyengar, L. & Krishna Rao, K. V. (1978). *J. Less-Common Met.* **60**, P41–P46.
Wagner, F. E., Sawicki, J. A., Friedel, J., Mandarino, J. A., Harris, D. C. & Cabri, L. J. (1994). *Can. Mineral.* **32**, 189–201.
Willis, B. T. M. & Pryor, A. W. (1975). *Thermal Vibrations in Crystallography*. Cambridge: Cambridge University Press.
Wood, I. G., Knight, K. S., Price, G. D. & Stuart, J. A. (2002). *J. Appl. Cryst.* **35**, 291–295.
Wyckoff, R. W. G. (1963). *Cryst. Struct.* 2nd ed., Vol. 1, pp. 7–83.
Yoshiasa, A., Kitahara, G., Tobase, T., Hiratoko, T., Hongu, H., Nakatani, T. & Murai, K. (2018). *Phys. Status Solidi B*, **255**, 1800050.
Yoshiasa, A., Nakatani, T., Nakatsuka, A., Okube, M., Sugiyama, K. & Mashimo, T. (2016). *Acta Cryst.* B**72**, 381–388.
Yoshiasa, A., Tokuda, M., Kitahara, G., Unoki, K., Isobe, H., Nakatsuka, A. & Sugiyama, K. (2021). *J. Cryst. Growth*, **574**, 126327.
Yoshiasa, A., Tokuda, M., Misawa, M., Shimojo, F., Momma, K., Miyawaki, R., Matsubara, S., Nakatsuka, A. & Sugiyama, K. (2019). *Sci. Rep.* **9**, 6275.
Young, D. P., Brown, C. L., Khalifah, P., Cava, R. J. & Ramirez, A. P. (2000). *J. Appl. Phys.* **88**, 5221–5224.
Zhang, J., Zhang, Y., Richmond, W. & Wang, H. P. (2010). *Int. J. Miner. Met. Mater.* **17**, 1–10.

electronic reprint